NASA Technical Memorandum 87052

Mechanism of Strength Degradation for Hot Corrosion of α-SiC

James L. Smialek and Nathan S. Jacobson
Lewis Research Center
Cleveland, Ohio

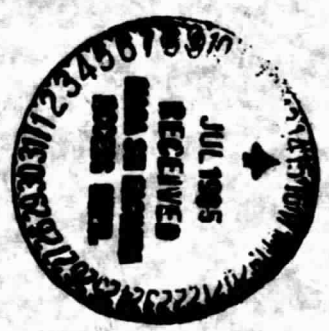

Prepared for
The Regional Meeting of the American Ceramic Society
San Francisco, California, October 28-31, 1984

NASA

MECHANISM OF STRENGTH DEGRADATION FOR HOT CORROSION OF α-SiC

James L. Smialek and Nathan S. Jacobson
National Aeronautics and Space Administration
Lewis Research Center
Cleveland, Ohio 44135

ABSTRACT

Sintered α-SiC was corroded by thin films of Na_2SO_4 and Na_2CO_3 molten salts at 1000 °C. This hot corrosion attack reduced room temperature strengths by as much as 50 percent. Strength degradation was proportional to the degree and uniformity of corrosion pitting attack as controlled by the chemistry of the molten salt. Extensive fractography identified corrosion pits as the most prevalent source of failure. A fracture mechanics treatment of the strength/pit depth relationship produced an average K_{IC} equal to 2.6 $MPa \cdot m^{1/2}$, consistent with published values.

E-2507

INTRODUCTION

The effects of hot corrosion attack on the mechanical properties of the high temperature structural ceramics, SiC and Si_3N_4, is a concern for combustion applications where impurities in the air and fuel might react and deposit as potentially corrosive molten salt films. Chemical reaction of this film with the ceramic could result in uniform material loss as well as selective localized attack or pitting. Loss of load bearing material, enlargement of the critical surface flaw size, or contamination of grain boundaries by the corrosive elements can result in degradation of the brittle fracture strength, decreased fracture toughness, and reduction of high temperature creep strength.

Justification for the generalities suggested above can be found in the literature described in the following brief chronological survey and as listed in Table I. As early as 1952 the "etching effect" of molten alkali carbonate salts on SiC at 1000 °C had been recognized.[1] This technique was successfully

used by Amelinckx and co-workers in 1960 to study dislocation structures in single crystal α-SiC.[2] This tendency for preferential attack at structural discontinuities and the effects on mechanical properties is a major consideration of the present paper.

Conventional high temperature corrosion studies on SiC and Si_3N_4, became more prevalent nearly 15 yr later when a number of crucible or deep melt studies were reported. The first of these found nearly complete dissolution of siliconized SiC heating elements in a melt of Na_2CO_3 after only 5 hr at 900 °C.[3] Crucible tests of hot pressed boron-doped SiC in $CaCl_2$ - CaF_2 - $CaSO_4$ melts produced high dissolution rates, 13 μm/min at 1000 °C and 60 μm/min at 1100 °C.[4] The rate was found to be linear with time and exhibited an Arrhenius relationship with temperature. Samples corroded at lower temperatures (822 °C) exhibited numerous 10 μm pits while higher temperature exposures (1152 °C) yielded more uniform surface dissolution. Different attack modes thus appear to be a possibility.

Pressureless sintered β-SiC, doped with carbon and boron, was exposed to Na_2SO_4, Na_2SO_4 + graphite, Na_2SO_4 + Na_2CO_3, and Na_2CO_3 melts at 900 °C.[5] This study also explored the effects of thin films of Na_2SO_4 (10 mg/cm^2) as might be expected in a gas turbine environment, but no excessive corrosion was observed as judged from the minimal weight gain changes observed. However 1 g melts of Na_2SO_4 in crucible tests did cause severe corrosion. This was attributed to the low P_{O_2} at the SiC-melt interface and to active oxidation through the formation of SiO vapor. The addition of basic salts (Na_2CO_3) to Na_2SO_4 shortened the induction period observed before the onset of accelerated oxidation or catastrophic corrosion. The following basic dissolution reaction was proposed:

$$SiO_2 + Na_2O = Na_2SiO_3 \text{ (liquid)} \qquad (1)$$

The addition of graphite also promoted excessive corrosion, produced bubbling in both the melt and liquid scale, and resulted in a very rough SiC-scale interface. A similar study found that deep, 50 g melts of Na_2SO_4 and Na_2SO_4 + NaCl rapidly consumed reaction sintered or hot pressed SiC and Si_3N_4 at 1000 °C.[6] NaCl melts alone did not appear to cause catastrophic corrosion. Electron microprobe studies of the Si_3N_4 revealed sodium, sulphur, and chlorine contamination ~40 μm beneath the Si_3N_4 surface.

Corrosion of reaction bonded Si_3N_4 was also studied by exposure to thin films of Na_2CO_3 (0.4 to 1.4 mg/cm^2) at 1000 to 1300 °C.[7] A linear rate of corrosion occurred for a limited time after which no further weight gains were observed. The maximum weight gain obtained before the reaction stopped was a linear function of the amount of salt deposit. Also the initial rate of corrosion increased with temperature in approximately an Arrhenius relationship. It was proposed that accelerated corrosion occurred in the presence of liquid sodium silicate phases until enough Si_3N_4 had been oxidized to produce a "healing layer" of solid tridymite. Indeed, estimates of the sodium and silicon concentrations in the scale at the time the reaction stopped agreed with the liquidus curve for the Na_2O - SiO_2 system. The linear rate of corrosion indicates that the process is not controlled by diffusion through a solid SiO_2 film and that no barrier exists to the transport of oxygen through the liquid silicate films.

Another study of reaction bonded Si_3N_4 proposed that nonprotective sodium silicate formation was the cause of hot corrosion attack by Na_2SO_4 or Na_2CO_3.[8] This study also used thin films (multiple applications of 5 mg/cm^2) and cyclic exposure to 1093 °C (1000 cycles, 5 min/cycle). The major crystalline phase was again tridymite and considerable surface roughening was observed after the corrosion product was easily crumbled and removed.

The studies mentioned above have documented the high degree of chemical reactivity between a number of SiC and Si_3N_4 ceramics in various molten salts. The following studies show that deleterious effects on mechanical properties occur after these ceramics were subjected to high temperature molten salt environments. In 1980, Bourne and Tressler reported results of crucible tests of hot pressed Si_3N_4 (144 hr) and reaction bonded Si_3N_4 (50 hr).[9] Exposures to deep melts of NaCl or NaCl + Na_2SO_4 were made at 1000 °C. This resulted in strength degradation of 30 to 60 percent, both at room temperature and at 800 to 1200 °C. Extensive pitting and material loss was reported for these materials after corrosion in the NaCl + Na_2SO_4 melt. The dramatic decrease in strength was consistent with calculations showing a significant increase in the critical flaw size, i.e., surface pits. Grain boundary weakening by Na, S, and Cl penetration was found to be a key factor in the degradation of high temperature strength.

Recently Becher reported the deleterious effects of 1220 °C coal slag exposures of hot pressed Si_3N_4 (MgO), Si_3N_4 (Y_2O_3), and SiC (Al_2O_3), as well as sintered SiC and siliconized SiC.[10] The slag deposits resulting from the combustion of fuel oil and powdered coal contained substantial amounts of SiO_2, Fe_2O_3, and Al_2O_3 with minor amounts of CaO, MgO, Na_2O, K_2O, and TiO_2. Strength reductions up to 65 percent were observed for Si_3N_4 in an acid slag. Basic slags caused higher rates of surface recession, but caused remarkably little strength degradation for two materials, Si_3N_4 (MgO) and sintered SiC. In general it was observed that oxide additives in the ceramics (MgO, Y_2O_3, or Al_2O_3) contributed to preferential attack via complex liquid silicate formation, and that gas evolution (bubble formation) also contributed to pitting, enhanced corrosion, and strength degradation. However, sintered α-SiC appeared to have a remarkably uniform scale-ceramic interface with only 10 μm deep pits after exposure to either basic or acidic slags. Strength retention

after removal of 20 μm of the corroded surface indicated that no deleterious penetration of contaminants occurred as found in earlier works.[6,9]

Another such study investigated the corrosion of sintered α-SiC by coatings of powdered coal slags.[12] Thin films (≤100 μm) of a basic slag resulted in the formation of a cristobalite passivating layer. Diametral compression C-ring tests found a strength increase after 24 or 168 hr exposures at 1250 °C. However, thick film corrosion (>2 mm) resulted in dissolution of SiO_2 layers, formation of Fe,Ni-silicides, and pitting attack. This pitting phenomenon was responsible for strength reductions from a value of ~350 MPa after 1 hr exposure to 300 MPa after 24 hr exposure at 1200 °C (or to 285 MPa at 1300 °C).

The morphology of corrosion products formed on various Si_3N_4 and SiC substrates was examined after being subjected to Na_2SO_4 thin films at 1000 °C.[11] Bubble formation and devitrification of protective SiO_2 scales were commonly found. Impurities in the ceramics (except aluminum) tended to increase the degree of hot corrosion attack as did the basicity of the corrosion condition. A similar study of Na_2SO_4 thin film (4 mg/cm^2) corrosion of hot pressed Si_3N_4 (Y_2O_3) found extensive corrosion product formation at 1000 °C after about a 5 hr incubation period.[13] Na_2SO_4 decomposition, followed by monitoring SO_2 evolution and chemical analysis of residual Na_2SO_4, was essentially complete after 30 hr. These results explained a significant minimum in the weight change curve at about 12 hr. Bubble formation in liquid $Na_2O{\cdot}xSiO_2$ scales accompanied this corrosion process.

Thus the present understanding of hot corrosion of SiC and Si_3N_4 materials is that under certain conditions severe attack can definitely occur and that this attack can degrade mechanical properties significantly. The key issues that arise from these studies are related to the chemical mechanism of attack and the mode of mechanical property degradation. The chemical mechanism issues

are: (1) the effects of the acid/base nature (oxide ion concentration) of the melt and the dissolution of protective SiO_2 films to form nonprotective liquid Na_2SiO_3; (2) the amount of salt deposit and the potential for active oxidation or increased Na_2SiO_3 conten' in the scale; (3) the role of additives and impurities in the ceramics which can either increase or decrease attack. All of these factors are important in determining the morphology of the corrosion product and attack front which in turn controls the nature of the mechanical property degradation, i.e., (1) general attack causing surface recession; (2) localized attack (pitting) causing an increase in the effective critical surface flaw size; and (3) grain boundary contamination causing deterioration of high temperature properties.

The purpose of the present program was to determine how hot corrosion attack of the type most likely to occur in a turbine engine could effect fast fracture strength. Thus thin salt films were used rather than the deep melts of a crucible test. Both Na_2SO_4 and Na_2CO_3 salts were used to study the effects of melt chemistry. Controlled SO_3 or CO_2 atmospheres were used to thermodynamically fix the oxide ion concentration in the salt at the start of the reaction. Since high temperature strength retention and near net shape fabrication capability are prime considerations for turbine hardware, commercially available pressureless sintered α-SiC having minimal additives was chosen for study.

Self-consistent chemical mechanisms of hot corrosion attack under the above conditions have already been elucidated in a companion study.[14] The distinguishing factor in this study was the use of quantitative chemical analysis of the scales by determining the composition of water soluble corrosion products (sodium sulfate and sodium silicate) and of HF soluble products (SiO_2). Weight gain data alone was found to be an ambiguous measure of corrosion because of losses due to the gaseous reaction-products, SO_2, CO,

CO_2, etc.[14] Over a 48 hr period, corrosion products 10 to 20 times as great as that occurring for simple oxidation were found. The basic salt, Na_2CO_3/CO_2, was found to form nonprotective liquid sodium silicates and solid tridymite phases as expected. However the acidic salt resulted in even greater corrosion due to the reaction of free carbon (~3 vol %) with Na_2SO_4 to form CO_2, liquid Na_2SiO_3, and tridymite. The morphology of the corrosion products formed under acidic conditions was that of gross eruptions from gas evolution which were also extremely friable. Under basic conditions, the scales were quite glassy and contained entrapped bubbles.

EXPERIMENTAL PROCEDURE

The material used in this study was injection molded and sintered α-SiC* which was doped with boron and carbon. The microstructure of this ceramic, shown in Fig. 1(a), consists basically of equiaxed ~10 μm grains and lenticular grains with an aspect ratio of about 10 to 1. A dispersion of porosity and inclusions, which were previously found to be titanium and 3 percent free carbon, is also evident.[14] Test specimens 0.25 by 0.5 by 2.5 cm were cut from 5.0 cm long as-received bars and ground on 45 and 15 μm diamond wheels. The microstructure after grinding, Fig. 1(b), indicates that surface damage (pullout) was on the order of 10 μm. This surface finish is believed to be more than adequate to produce fracture strength values which are not controlled by surface grinding flaws. The basis for this conclusion lies in a previous study which found no strength increases for Si_3N_4 when polished to a degree finer than 600 grit (i.e., ~15 μm surface finish).[15]

The corrosion test procedure and chemical analysis scheme has been described previously in detail.[14] In general, the specimens were heated to 200 °C and sprayed with 2 to 3 mg/cm^2 films of Na_2SO_4 or Na_2CO_3 from aqueous

---

*Hexaloy, Carborundum Co., ca. 1977.

salt solutions. Three salt/gas exposure systems were chosen for study, i.e., Na_2SO_4/0.1 percent SO_2 in O_2, Na_2SO_4/Air, and Na_2CO_3/0.1 percent CO_2 in O_2. The first system is close to a situation which might be encountered in a gas turbine burning high sulfur fuels. The second simulates the environment of a gas turbine burning low sulfur fuels. Finally the third system provides a basic salt chemistry known to react directly with SiO_2.

Two sets of samples for strength testing were produced from each group of corroded specimens. One set was directly sanded using 325 and 600 grit SiC emery paper, followed by 15 μm diamond grinding. This was done to produce the flat surface needed for strength testing because the corrosion products were often quite nonuniform.[14] (Surface irregularities as large as 0.5 mm were measured which would have otherwise resulted in a serious misalignment of the bend test fixture and erroneous values of measured strength.) Polishing was terminated after producing a flat surface, but before reaching the SiC substrate. This allowed a thin layer of corrosion product to remain on the ceramic before strength testing. The other set of specimens was prepared for bend testing by removing all the corrosion products, first by water dissolution, then by 10 percent HF - H_2O dissolution at ~90 °C for 2 hr in each solution.

Control samples of uncorroded as-ground SiC were also subjected to this HF dissolution treatment. While very little dissolution was observed from chemical analysis of the solution, a 25 percent strength decrease was measured. Similarly after 48 hr of oxidation at 1000 °C with no salt coating HF dissolution of the scales produced a 23 percent strength decrease. These decreases were statistically significant at the 95 percent confidence level. Thus corroded samples subjected to the HF treatment were not used in the measurement of strength degradation to avoid this complicating factor. Specimens were stressed to fracture in 4-point bending using a loading rate of

0.05 cm/min, an outer span of 1.90 cm and an inner span of 0.95 cm. The fracture surfaces were examined by optical microscopy, scanning electron microscopy, and electron microprobe for identification and characterization of corrosion-induced flaws (failure origins). Strengths were calculated from the equation:

$$\sigma = \frac{3/4\ Pl}{wt^2} \qquad (2)$$

where P is the applied load at failure, l is the outer span, w is specimen width, and t is specimen thickness. The original specimen dimensions were used in these calculations even though some SiC had been converted to a corrosion scale and even though some of the polished scale remained on the samples during strength testing. This procedure was adopted to allow the effects of any surface recession to be reflected in the load carrying capability one would predict using original specimen dimensions (engineering design strength). In reality both the surface recession and amount of residual scale were minimal (<20 μm) so that no significant effect on strength arose from these factors. A minimum of five specimens were run per corrosion condition.

RESULTS

Strength Degradation and Surface Recession

The average amount of corrosion product in terms of weight change per unit area, $\Delta w/A$, for the three corrosion treatments and for simple air oxidation was determined previously by chemical analyses of dissolved scales and is shown in Table II.[14] The scale thickness, Δt_e, can be estimated from this quantity if a density of ~2.65 gm/cm^3 is assumed for an SiO_2 scale. The actual scale thickness, Δt_m, was also determined by physically measuring the change in specimen thickness. That is, $\Delta t_m = (t_c - t_o)/2$ where t_c = the apparent specimen thickness after corrosion and t_o = the initial thickness.

It is readily apparent in Table II that $\Delta t_m > \Delta t_e$, especially for the case of Na_2SO_4/SO_3 corrosion. This is due to the fact that these corrosion products were extremely rough. Only the Na_2CO_3/CO_2 condition produced $\Delta t_m \approx \Delta t_e$, as expected from the uniform glassy scales produced by this treatment. No thickness changes could be detected for simple oxidation.

Also shown in Table II are surface recession values obtained after polishing the scales, $(t_o - t_p)/2$, where t_p is the specimen thickness after polishing the corroded specimen to a 15 μm finish. These values were generally low (<10 μm) so that any strength reduction due to surface recession should also be minimal. For example, a surface recession of 20 μm would result in a strength loss of only 1 percent for samples with a 2.2 mm thickness. A similar conclusion was reached for samples whose scales were removed by HF dissolution. The recession value, $(t_o - t_d)/2$, where t_d is the specimen thickness after HF treatment, was found to be on the order of only 15 μm.

The average flexural strength (modulus of rupture, MOR) of the corroded samples is shown in Fig. 2 along with the values for the as-received material. All the samples were tested in the 15 μm diamond polished condition. The individual data points have also been plotted to give a realistic picture of the spread in the MOR data and the overlap between treatments. The most severe strength degradation (49 percent) occurred in the case of Na_2SO_4/SO_3, followed by 38 percent for Na_2SO_4/Air, and 13 percent for Na_2CO_3/CO_2. The as-received strength value of 409 MPa compares reasonably well with published values for this material of 335, 365, and 425 MPa.[16-18]

Because large standard deviations were observed (±20 percent), a statistical comparison of the data was required to make a conclusive statement on the degree of strength degradation. The pertinent data is shown in Table III. The Student's t-distribution was used to find the 95 percent confidence intervals of the mean $\bar{\sigma}_f$ values. The 95 percent confidence

interval for as-received strength was above those for the corrosion treatments, except for the Na_2CO_3/CO_2 case which showed a slight overlap. The change in strength after corrosion, $\Delta\bar{\sigma}$, and the 95 percent confidence interval of $\Delta\bar{\sigma}$ were determined by means of the t-statistic to test the significance of the strength reductions. For the Na_2SO_4/SO_3 and Na_2SO_4/Air treatments the 95 percent confidence interval of $\Delta\bar{\sigma}$ was at least 100 MPa and indicated that these treatments caused a significant strength reduction. However the $\Delta\bar{\sigma}$ interval for Na_2CO_3/CO_2 corrosion could be less than zero at some finite probability (2.5 percent). Therefore this treatment did not reduce the mean strength significantly according to this t-test.

Attack Morphology

Although the amount of corrosion product was up to twenty times that of simple oxidation (table II), this could still not account for enough uniform surface recession to cause this degree of strength reduction. The explanation lies in the morphology of the corrosion attack rather than in the amount. From the previous study it had been concluded that the principal mechanism of attack was through pitting.[14] This effect is shown in Fig. 3 for Na_2SO_4/SO_3 (acidic) corrosion. Here the widespread uniform pitting of a severe nature is readily apparent after the scale had been removed by the HF treatment.** Some measure of the severity of the pitting attack was obtained from stereopair measurements across the trace designated as X-X in Fig. 3(b). This profile shown in Fig. 4 indicates a pit depth of at least 70 μm, with deeper pitting suggested but not resolvable from the micrographs.

**It was previously demonstrated that no change in morphology or material loss occurred when as-received SiC was HF treated, and that complete scale removal by HF dissolution was indeed accomplished for corroded SiC samples.[14]

The SiC morphology after Na_2CO_3/CO_2 (basic) corrosion and scale dissolution in HF is shown in Fig. 5. Figure 5(a) shows a coarse cellular network of corrosion pits which is nonuniformly distributed over the sample surface. The pits comprising these cell boundaries (Fig. 5(b)) exhibit the honeycomb structure similar to the Na_2SO_4/SO_3 case. The region at the center of the cells, however, is quite flat by comparison (Fig. 5(c)). These areas also exhibit ~0.1 μm grain boundary films and partially consumed particles (arrows). Both of these features are believed to be excess carbon (graphite), as found in previous studies by windowless SEM/EDS, electron microprobe, and STEM/EELS.[14,19]

The Na_2SO_4/Air treatment can neither be classified as acidic or basic because its SO_3 equilibrium pressure is undefined.[14] However it was chosen for study because it produces attack morphologies and product chemistries similar to those obtained in a burner rig study, which is a closer approximation to the environment of a gas turbine.[20] This attack morphology shown in Fig. 6 is somewhat similar to that for the Na_2CO_3/CO_2 case in that considerable nonuniformity in the degree of surface pitting was produced. Although no distinct cell patterns were observed on this sample, some areas showed deeper pits, (arrow in Fig. 6(a)). This pit had a very granular nature (Fig. 6(b)) as did the surrounding areas even though they were quite flat (Fig. 6(c)). Other samples were found to have the thin (~0.1 μm) grain boundary films identical to those found in the Na_2CO_3/CO_2 case.

It is clear from the last three figures that the attack morphology can vary considerably depending on the corrosion conditions. One feature believed to be crucial in determining the degree of strength degradation is the size of the pit and the frequency of occurrence of pits of a given size. An attempt to quantify such a description of the attack morphology is shown in Fig. 7. These curves (histograms) were obtained by measuring the diameters of all the pits observed in a total area of ~0.1 mm^2. This data was arranged in order

of ascending diameter and the pit size frequency versus diameter was determined from the number of pits (ΔN) occurring in successive size intervals (ΔD) of 4 μm. The conclusion is that the Na_2SO_4/SO_3 treatment produced the highest numbers of large pits, followed by Na_2SO_4/Air, and then Na_2CO_3/CO_2. If it is assumed that the pit depth is roughly commensurate with the pit diameters, then the Na_2SO_4/SO_3 case should have the most severe strength degradation due to the formation of the deepest pits as critical surface flaws. Next in the sequence should be Na_2SO_4/Air, followed by Na_2CO_3/CO_2, as indeed was the case for the actual strength measurements.

The most important information regarding pit sizes would be the probabilities of the very large pits occurring, as these pits constitute the "weakest link" controlling the fracture stress. However, obtaining pit size data on these was the most difficult since they were the least populous. An alternative presentation of the pit frequency data is shown in Table IV. The pits likely to compete with naturally existing flaws for controlling fracture should have depths $\geq$20 μm.[16] Of the largest pits measured, Na_2SO_4/SO_3 samples had 90 pits/mm^2 as compared to only 4 pits/mm^2 for Na_2CO_3/CO_2 samples. This trend can be expected to exist for pits $\geq$40 μm, but with much smaller pit frequencies. The sample surface area under the maximum tensile stress was ~100 mm^2. Thus the Na_2SO_4/SO_3 samples were expected to contain many large pits with $D \geq 40$ μm and produced reproducibly low strengths, while the Na_2CO_3/CO_2 samples may have had an occasional large pit which resulted in widely varying strengths (226 to 474 MPa).

Fractography

The above discussion has raised the hypothesis that corrosion pitting caused serious strength reductions proportional to the size and frequency of the pits. The following fractographic study (SEM) will present typical

examples of the flaws that actually caused failure in order to verify this hypothesis.

Often the fracture sections exhibited optically reflective mirror-like regions which contained directional fracture lines pointing to the fracture origin at the tensile surface. It is believed that these reflective regions are large, plate-like SiC grains (as in Fig. 1(a)) which cleaved transgranularly. Such features had been observed previously in fracture sections of the same material and were occasionally found to be failure origins as well.[21] In many instances these mirrors existed near the fracture origin and crack lines within the mirror eminated radially from the origin. An example is shown in Fig. 8(a) for a Na_2SO_4/SO_3 sample whose scale was polished to a 15 μm finish before fracture. The flaw was indeed a corrosion pit still filled with oxide (Fig. 8(b)) which contained numerous pores. A rim of porosity in the SiC also existed near the periphery of the pit as indicated by the arrows. The smooth internal surfaces of the scale porosity, Fig. 8(c), was consistent with the previous observation of gas evolution and bubbles entrapped in the scale.

The material in the fracture origin was conclusively identified as oxide by electron microprobe oxygen mapping. However the resolution of this technique was not high enough to identify the exact scale-SiC interface. This was accomplished by HF dissolution of the corrosion products and reexamination, as shown in Fig. 9 (detail of the right edge of the pit in Fig. 8(b) before and after dissolution). It can readily be seen that the brighter regions in relief of Fig. 9(a) were part of the scale and that the cavity here was a gas bubble in the scale which formed only a few micrometers from the interface. Thus bubble formation is likely to play a key role in the pitting mechanism. The SiC in contact with the oxide showed a very rough surface texture after scale removal (Fig. 9(b)).

The fractographs of a Na_2SO_4/SO_3 treated sample whose scale had been removed by HF dissolution are shown in Fig. 10. Again radial crack lines were found to eminate from the origin (Fig. 10(a)). At higher magnification, (Fig. 10(b)) the familiar honeycomb pit structure was observed at the fracture origin, proving again that a corrosion pit initiated failure. The details of the corrosion front (arrow in Fig. 10(b)) is shown in Fig. 10(c). Connected intergranular porosity can be seen to form ~10 μm ahead of the pit. This implies that selective oxidation/corrosion of the grain boundaries is another important factor in the overall pitting mechanism. In this case the pit depth including the grain boundary attack region was found to be ~133 μm.

Fractured specimens previously corroded in Na_2CO_3/CO_2 also exhibited corrosion pits as the common failure origin. An example of such a pit is shown in Fig. 11. A small flat mirror-like feature was located at the origin; within this feature and beyond were radial crack lines having the corrosion pit as the focal point (Figs. 11(a) and (b)). The top (tensile) surface of the specimen shows a number of ~20 μm entrapped bubbles which had been exposed by the polishing treatment. The scale-SiC interface shown in Fig. 11(c) exhibited a smaller amount of porosity than the Na_2SO_4/SO_3 samples. The position of the exact interface (arrows in Figs. 11(c) and (d)) was determined by removing the scale through HF dissolution. This treatment revealed the pocked-marked structure typical of the cell boundary pitted regions of the corroded surfaces (Fig. 5(b)). It should also be pointed out that the interface is much smoother and the pit much shallower (~45 μm) than those observed for Na_2SO_4/SO_3 corrosion. No indication of deep gain boundary attack was found.

A typical fracture origin for the Na_2SO_4/Air case is shown in Fig. 12 for a specimen whose scale was removed by HF dissolution. The identifying radial crack lines pointed to a corrosion pit at the origin (Fig. 12(a)). Some relatively deep penetrations were apparent (Fig. 12(b)), but the preferential

grain boundary attack of the Na_2SO_4/SO_3 case did not occur. The pit-SiC interface (arrow) is shown at high magnification in Fig. 12(c). The interior of the pit reveals the faceted granular nature of the attack as well as the finely etched surfaces of the exposed grains.

Pit Size, Fracture Strength, and Fracture Toughness

The fractographic analysis revealed that in the majority of cases, the fracture origins were surface corrosion pits (100 percent of the fractography specimens for Na_2SO_4/SO_3, 50 percent for Na_2CO_3/CO_2, and 67 percent for Na_2SO_4/Air). Most of the fracture origins in the remaining cases could not be identified, although some were associated with a surface processing defect. Thus the fracture strength was predominantly controlled by the corrosion pitting phenomenon.

Since brittle fracture strength is dependent on the size of the critical flaw, there should ideally be a relationship between strength, σ_f, and the flaw (pit) depth, a, according to the relation for semicircular flaws:

$$\sigma_f = \frac{Z}{Y} \frac{K_{IC}}{\sqrt{a}} \tag{3}$$

where Z is the flaw shape parameter (elliptical integral) and Y is a geometric factor.[22] Accordingly, the fracture strength is plotted as a function of pit depth in Fig. 13 for all the cases where a corrosion pit was successfully identified as the failure origin. Despite the considerable scatter, the expected overall trend of decreasing strength with increasing pit depth was apparent.

The scatter could be reduced somewhat by taking into account the variable pit geometries (a/c ratios) which result in different values of Z/Y. These terms have been accurately determined by the finite element analysis of Newman and Raju.[23] This analysis of the data resulted in an average K_{IC} of 2.64 ± 0.43 MPa$\cdot$m$^{1/2}$. The fracture toughness was also estimated from the

approximation given by Bansal[22] for semi-elliptical surface cracks having $0.2 < a/c < 3$:

$$\sigma_f \cong 0.750 \frac{K_{IC}}{(ac)^{1/2}} \quad (4)$$

This relation takes into account both axes of the flaw, is very convenient to use, and is said to result in no more than a 5 percent error in K_{IC}. A value of K_{IC} was thus estimated from Eq. 4 to be 2.87 ± 0.46 MPa•m$^{1/2}$, in reasonable agreement with the value obtained from the Newman-Raju technique.

Treatment of the corrosion pits as critical flaws is of course predicated on the assumption that they can be approximated as semicircles or ellipses having atomically sharp circumferential cracks. Since the flaw geometry and sharpness was subject to large variations, the residual scatter in K_{IC} calculations was unavoidable. Another source of variability could be the interaction of corrosion pits with large grains during the fracture process. Nonetheless the agreement of this K_{IC} value to the following published values strengthens the argument that corrosion pitting controlled bend strength. Similar variations in K_{IC} values were obtained in attempting to describe fracture strength as a function of naturally occurring processing flaws.[24] This study found the "σ_f" and "a" values to be grouped within bands predicted for K_{IC} = 2.0 to 2.8 MPa•m$^{1/2}$, which is quite similar to the range found in the present study. Presumably the absence of detailed information on the exact dimensions of unobservable cracks in the vicinity of the processing flaws precludes a more accurate analysis. The use of controlled indentation flaws produced K_{IC} values near 2.5 MPa•m$^{1/2}$ which is within the range of the values obtained from the corrosion pit or processing flaw analyses.[24]

A well-regarded toughness measurement, the chevron notch short bar technique (CNSB), was used to determine $K_{IC} = 2.79 \pm 0.17$ MPa•m$^{1/2}$ for the same

material (vintage ca. 1982).[25] The statistical t-test proved that this value was indistinguishable from the 2.64 MPa•$m^{1/2}$ value obtained from corrosion specimens at the 95 percent confidence level. Other similar fracture toughness values determined by microhardness indentation (MI), double cantilever beam (DCB), and controlled flaw (CF) bend tests are also shown in Table V.

The factor Z/Y in Eq. (3) can be determined to be 0.785 from Ref. 22 or 0.783 from Ref. 23 for a semicircular crack (a/c = 1). Thus the "σ_f" versus "a" behavior can be predicted for various K_{IC} values as shown by the lines in Fig. 13. The 2.64 MPa•$m^{1/2}$ curve falls near the middle of all the data and is consistent with the observation that the average a/c = 0.96±0.45, i.e., near unity. The curve predicted for K_{IC} (CNSB) = 2.79 MPa•$m^{1/2}$ and the curve measured by controlled semicircular flaws also fall well within the scatter band of Fig. 13.[16] This latter curve was used to calculate a K_{IC} value of 2.36 MPa•$m^{1/2}$. The agreement between these curves or equivalently between the fracture toughness values is consistent with the conclusion that corrosion pitting controlled the fracture strengths and was responsible for the observed strength degradation. Also, the deepest pits causing failure were found for the Na_2SO_4/SO_3 samples and were 90 μm on average, resulting in an average strength of 213 MPa. The fractography data for Na_2CO_3/CO_2 and Na_2SO_4/Air was sparse by comparison. However it was still found that the average pit depths causing failure were considerably smaller, 54 and 40 μm, and the average strengths were accordingly higher, 332 and 307 MPa, for Na_2CO_3/CO_2 and Na_2SO_4/Air, respectively.

Another point suggested by this analysis is that the room temperature value of K_{IC} was not significantly degraded by thin film molten salt corrosion. This is in contrast to more severe crucible tests of hot pressed Si_3N_4 in NaCl or NaCl + Na_2CO_4 melts where K_{IC} was generally reduced at both ambient and elevated temperatures.[15]

DISCUSSION

The results reported here emphasize the importance of corrosion pit formation to the strength degradation of SiC. The diameter, depth, and frequency of the pits were shown to vary with the corrosive salt used and atmosphere. These variations could also account for the general trend in the strength reductions and for the wide spread in strengths for certain corrosion conditions. The fracture strengths of individual specimens were also correlated to the size of the pit actually causing failure (from fractography) according to a fracture toughness formalism which predicted a K_{IC} value consistent with literature values.

The task now at hand is to put forth an explanation which describes the mechanism of corrosion pitting as a function of the chemical environment. This deeper understanding would allow some predictive capability for corrosion under different salts, thicker films, longer times, and the effects of various impurities and dopants in SiC. Unfortunately a completely satisfactory picture of pitting eludes us at present. A few comments are nevertheless appropriate. First, the process does not appear to be correlated with regions of high impurity content (C, Ti, K) because the size of the pits was much larger than the scale of any chemical inhomogenity. Furthermore the variation in pit size and frequency with the corrosion treatment is not consistent with a phenomenon based wholly on material homogeneity.

Another relevant observation is the widespread gas evolution indicated by the large eruptions for Na_2SO_4/SO_3 samples and entrapped gas bubbles for Na_2CO_3/CO_2 and Na_2SO_4/Air samples. The porosity at the scale-SiC interface observed in fracture sections was another manifestation of gas evolution. It is believed that this is important for pitting because of the common observation that pits are associated with gas bubbles formed in SiO_2 scales on SiC.[10,27]

Excess carbon in α-SiC played a key role in Na_2SO_4/SO_3 corrosion by making the dissolution of SiO_2 by Na_2SO_4 thermodynamically favorable.[14] This viewpoint is consistent with the large eruptions and selective attack of graphite grain boundary inclusions under Na_2SO_4/SO_3 conditions. By comparison, large eruptions and deep grain boundary attack did not occur under the two other conditions. Here carbon-rich films and inclusions could be found which were only partially consumed at the interface.

Differences in gas evolution can be seen from the reactions put forth describing the chemical mechanisms of corrosion for Na_2SO_4/SO_3 (Eq. (5)) and Na_2CO_3/CO_2 (Eq. (6)):

$$SiO_2 + Na_2SO_4 + 2C + 3/2\ O_2 = Na_2SiO_3 + 2CO_2 + SO_2 \quad (5)$$

$$SiO_2 + Na_2CO_3 = Na_2SiO_3 + CO_2 \quad (6)$$

These reactions show the direct reaction of carbon with Na_2SO_4 and the formation of three times as much gaseous product as the Na_2CO_3/CO_2 case. This may account for the more violent reaction and greater pitting. A previous study found that carbon additions to Na_2SO_4 resulted in accelerated corrosion and roughening of β-SiC.[5] However, active oxidation by SiO formation was suggested as the cause of corrosion rather than excessive CO_2 formation. The detailed mechanism by which gas evolution might promote pitting is not clear and is the focus of current research.

The degradation in strength due to pitting is similar to the findings of crucible and combustion rig testing of SiC and Si_3N_4 in fused salt or coal slag melts.[9,10] Thus corrosion pitting of silicon-based ceramics is likely to be a general mechanism of degradation. The correlation of fracture strengths with the size of the actual pits causing failure found in this study provides a quantitative perspective of this degradation in the present study. However this cannot be used as a precise predictive technique without further

understanding because of the irregularities in pit geometry, the uncertainty regarding the sharpness of the pit front, and the wide variations in pit sizes.

This work and the companion study[14] have shown that the three corrosion conditions all substantially corroded α-SiC, but still produced noticable differences in the amount of corrosion products, the morphology of the scales, and the degree of pitting and strength degradation. This emphasizes the need to identify what conditions might be expected for turbine exposures, presuming NaCl ingestion and typical levels of sulfur impurities in the fuel. Although no actual engine corrosion tests have been performed, a simulated environment in a burner rig (1000 °C, 4 atm, 13.5 hr) produced scale chemistries and morphologies, pitting attack, and strength reductions that closely resembled those observed in Na_2SO_4/Air furnace exposures.[20]

SUMMARY AND CONCLUSIONS

Hot corrosion of sintered α-SiC produced average strength reductions of 49, 38, and 13 percent for Na_2SO_4/SO_3, Na_2SO_4/Air, and Na_2CO_3/CO_2 thin films, respectively. These strength losses were statistically significant at the 95 percent confidence level, except for the Na_2CO_3/CO_2 case. This was due in part to the large spread in strength data for that treatment. Examination of the attack morphology established that frequent large pits occurred on Na_2SO_4/SO_3 samples which accounted for the dramatic strength decrease. At the other extreme, shallower, less numerous pits occurred on Na_2CO_3/CO_2 samples resulting in higher overall strengths as well as the wide spread in strength values.

Detailed fractography conclusively identified corrosion pits as the most prevalent cause of failure for all three corrosion conditions. This technique also revealed features important to the pitting process such as interface bubble formation and selective grain boundary attack. An analysis of the relationship between pit size and strength produced an average value of

fracture toughness, K_{IC}, equal to 2.6 MPa•$m^{1/2}$. This is in good agreement with independently determined values of 2.3 to 2.8 MPa•$m^{1/2}$ and is consistent with the hypothesis that pitting controls the room temperature strength of SiC corroded by thin films of molten salts.

REFERENCES

[1] F.H. Horn, Philos. Mag., 1952, 43, 1210-1213.

[2] S. Amelinckx; G. Strumane; W.W. Webb, J. Appl. Phys., 1960, 31, 1359-1370.

[3] E. Buchner; O. Rubisch, In "Silicon Carbide - 1973"; R.C. Marshall; J.W. Faust, Eds., University of South Carolina Press, Columbia, SC, 1974, pp. 428-434.

[4] R.H. Arendt; M.J. Curran, In "Metal-Slag-Gas Reactions and Processes"; Z.A. Foroulis; W.W. Smeltzer, Eds., The Electrochemical Society, Pennington, NJ, 1975, pp. 636-647.

[5] D.W. McKee; D. Chatterji, J. Am. Ceram. Soc., 1976, 59, 441-444.

[6] R.E. Tressler; M.D. Meiser; T. Yonushonis, J. Am. Ceram. Soc., 1976, 59, 278-279.

[7] M.I. Mayer; F.L. Riley, J. Mater. Sci., 1978, 13, 1319-1328.

[8] M. Levy; J.J. Falco, Am. Ceram. Soc. Bull., 1978, 57, 457-458.

[9] W.C. Bourne; R.E. Tressler, Am. Ceram. Soc. Bull., 1980, 59, pp. 443-446, 452.

[10] P.F. Becher, J. Mater. Sci., 1984, 19, 2805-2814.

[11]J.R. Blachere; F.S. Pettit, "High Temperature Corrosion of Ceramics," DOE/ER/10915-3, Univ. of Pittsburgh, 1984.

[12]M.K. Ferber; J. Ogle; V.J. Tennery; T. Henson, J. Am. Ceram. Soc., 1985, 68, 191-197.

[13]W.J. Fielder, "Oxidation and Hot Corrosion of Hot-Pressed Si_3N_4 at 1000 °C," NASA TM-86977, 1985.

[14]N.S. Jacobson; J.S. Smialek, "Hot Corrosion of Sintered α-SiC," Accepted by J. Am. Ceram. Soc.

[15]W.C. Bourne; R.E. Tressler, In "Fracture Mechanics of Ceramics, III"; R.C. Bradt; D.P.H. Hasselman; F.F. Lange, Eds., Plenum Press, New York, 1978, pp. 113-124.

[16]R.K. Govila, J. Mater. Sci., 1984, 19, 2111-2120.

[17]P.F. Becher, J. Am. Ceram. Soc., 1983, 18, C-120 to C-121.

[18]R.C. Bradt, "The Impact Resistance of SiC and Other Mechanical Properties of SiC and Si_3N_4," NASA CR-165325, 1984.

[19]N.J. Tighe, In "Microbeam Analysis - 1984"; A.D. Romig, Jr; J.I. Goldstein, Eds., San Francisco Press, 1984, pp. 127-130.

[20]N.S. Jacobson; C.A. Stearns; J.L. Smialek, "High Pressure Burner Rig Corrosion of α-SiC," Submitted to J. Am. Ceram. Soc.

[21]J.W. Adams; D.C. Larsen, "Evaluation of Corrosion-Erosion Behavior of Various Ceramic Materials," AFWAL-TR-84-4067, Air Force Wright Aeronautical Lab, OH, 1984.

[22]G.K. Bansal, J. Am. Ceram. Soc., 1976, 59, 87-88.

[23]J.C. Newman; I.S. Raju, "Analysis of Surface Cracks in Finite Plates Under Tension or Bending Loads," NASA TP-1578, 1979.

[24]S.G. Seshadri; M. Srinivasan, J. Am. Ceram. Soc., 1981, 64, C69-C71.

[25]J.H. Wiegand, Private Communication, NASA Lewis Research Center, 1985.

[26]K.T. Faber; A.G. Evans, J. Am. Ceram. Soc., 1983, 66, C94 to C96.

[27]D.M. Mieskowski; T.E. Mitchell; A.H. Heuer, J. Am. Ceram. Soc., 1984, 67, C17 to C18.

TABLE I. - CHRONOLOGICAL SURVEY OF SiC AND Si_3N_4 HOT CORROSION STUDIES

Date	Reference	Materials	Corrodants	Technique	Observations
1952	(1) Horn	S.C. α-SiC	Na_2CO_3 1000 °C	Crucible	Dislocation etch pitting
1960	(2) Amelinckx, Strumane, Webb	S.C. α-SiC	Na_2CO_3 1000 °C	Crucible	Dislocation etch pitting
1974	(3) Buchner, Rubisch	SiC (Si)	Na_2CO_3 ≤900 °C	Crucible	Complete dissolution
1975	(4) Arendt, Curran	H.P. SiC (B)	Ca (F, Cl)$_2$ + $CaSO_4$ ≤1100 °C	Crucible	Severe etching, Arrhenius behavior
1976	(5) McKee, Chatterji	β-SiC (B_4C)	Na_2SO_4 (+ C, Na_2CO_3) 900 °C	Crucible, thin film	Active corrosion promoted by deep basic melts and carbon
1976	(6) Tressler, Meiser, Yonushonis	R.B. SiC R.B. Si_3N_4 H.P. SiC (Al_2O_3) H.P. Si_3N_4 (MgO)	Na_2SO_4 (+ NaCl) 1000 °C	Crucible	Rapid consumption in Na_2SO_4 - containing melts; Na, S, Cl grain boundary penetration
1978	(7) Mayer, Riley	R.B. Si_3N_4	Na_2CO_3 ≤1300 °C	Thin film	Initial fast growth of liquid Na_2SiO_3; reaction stops when SiO_2 formed
1978	(8) Levy, Falco	R.B. Si_3N_4	Na_2CO_4, Na_2CO_3 1093 °C	Thin film	Friable corrosion products; extensive surface roughening
1980	(9) Bourne, Tressler	R.B. Si_3N_4 H.P. Si_3N_4 (MgO)	NaCl (+ Na_2SO_4) 1000 °C	Crucible	Severe (~50 percent) strength reduction, pitting, and Na, S, Cl penetration
1984	(10) Becher	H.P. SiC (Al_2O_3) α-SiC (B, C) α-SiC (Si) H.P. Si_3N_4 (MgO) H.P. Si_3N_4 (Y_2O_3)	Coal slags: SiO_2 + $(Al,Fe)_2O_3$ + (Ca,Mg)O + $(Na,K)_2O$ 1200 °C	Combustion product deposition	Faster corrosion in basic slags: more strength degradation (up to 65 percent) due to pitting in acidic slags
1984	(11) Blachere, Pettit	CVD Si_3N_4 H.P. Si_3N_4 (Y_2O_3) S.C. SiC CVD SiC H.P. SiC (Al_2O_3)	Na_2SO_4 1000 °C	Thin film	Bubble formation; spherolitic devitrification and cracking of SiO_2 layer

TABLE I. - (Continued)

Date	Reference	Materials	Corrodants	Technique	Observations
1985	(12) Ferber, Ogle, Tennery, Henson	α-SiC (B, C)	Basic coal slag (as in Ref. 10) 1200-1300 °C	Thin, thick slurry coatings	Pitting, surface recession, and strength reduction only for films >100 μm thick.
1985	(13) Fielder	H.P. Si_3N_4 (Y_2O_3)	Na_2SO_4 1000 °C	Thin film	Incubation period, massive liquid $Na_2O \cdot xSiO_2$ scales with bubbles, SO_2 evolution.
1985	(14) Jacobson, Smialek	α-SiC (B, C) H.P. SiC (Al_2O_3) S.C. SiC	Na_2SO_4, Na_2CO_3 1000 °C	Thin film	Acidic attack severe only in presence of carbon, basic attack of all materials; severe pitting; quantitative analysis found SiO_2/Na_2SiO_3 = 4/1 (basic case) and 10/1 (acidic case)

TABLE II. - COMPARISON OF THICKNESS CHANGES DUE TO HOT CORROSION OF α-SiC
[1000 °C, 48 hr.]

Corrosion conditions	$\Delta W/A$	$\Delta t_e = \Delta W/A\rho$	$\Delta t_m = (t_c - t_o)/2$	$R_p = (t_o - t_p)/2$	$R_d = (t_o - t_d)/2$
	Total scale weight, mg/cm^2	Estimated scale thickness, μm	Measured scale thickness, μm	Polishing recession, μm	HF dissolution recession, μm
Na_2SO_4/SO_3	12.14±0.98	46±4	202±55	-2±5	9±4
Na_2CO_3/CO_2	6.18±0.27	24±1	25±14	7±6	15±19
Na_2SO_4/AIR	5.75±1.30	22±5	69±41	6±5	-4±14
Oxidation	0.47±0.34	2±1	------	----	-----

TABLE III. - EFFECT OF HOT CORROSION ON ROOM TEMPERATURE BEND STRENGTH
[1000 °C, 48 hr exposure; samples polished to 15 μm finish.]

Salt corrodant	Average strength $\bar{\sigma}_f$, MPa	Standard deviation S, MPa	Sample size, n	95 percent confidence interval of $\bar{\sigma}_f$, MPa	$\Delta\bar{\sigma} = \bar{\sigma}_{A.R.} - \bar{\sigma}_f$	95 percent confidence interval of $\Delta\sigma$	Significant strength reduction
As-received	409	62	15	443,375	---	-------	-
Na_2SO_4/SO_3	207	72	5	296,118	202	271,133	✓
Na_2CO_3/CO_2	355	70	14	395,315	44	94, -6	X
Na_2SO_4/AIR	251	45	8	288,213	158	210,106	✓

TABLE IV. - PIT SIZE DISTRIBUTIONS FOR CORRODED α-SiC
[Number of pits per 1 mm^2 area.]

	Dia <10 μm	10 μm < Dia <20 μm	Dia >20 μm
Na_2SO_4/SO_3	1880	620	90
Na_2CO_3/CO_2	2280	30	4
Na_2SO_4/AIR	17280	120	6

TABLE V. - FRACTURE TOUGHNESS VALUES FOR α-SiC

Technique	K_{IC} ($MPa \cdot m^{1/2}$)	Reference
Pits	2.64±0.43	This study
CNSB	2.79±0.17	Wiegand (25)
MI	2.3	Faber, Evans (26)
DCB	2.5	Faber, Evans (26)
CF	2.36	Govila (16)
CF	2.5	Seshadri, Srinivasan (24)

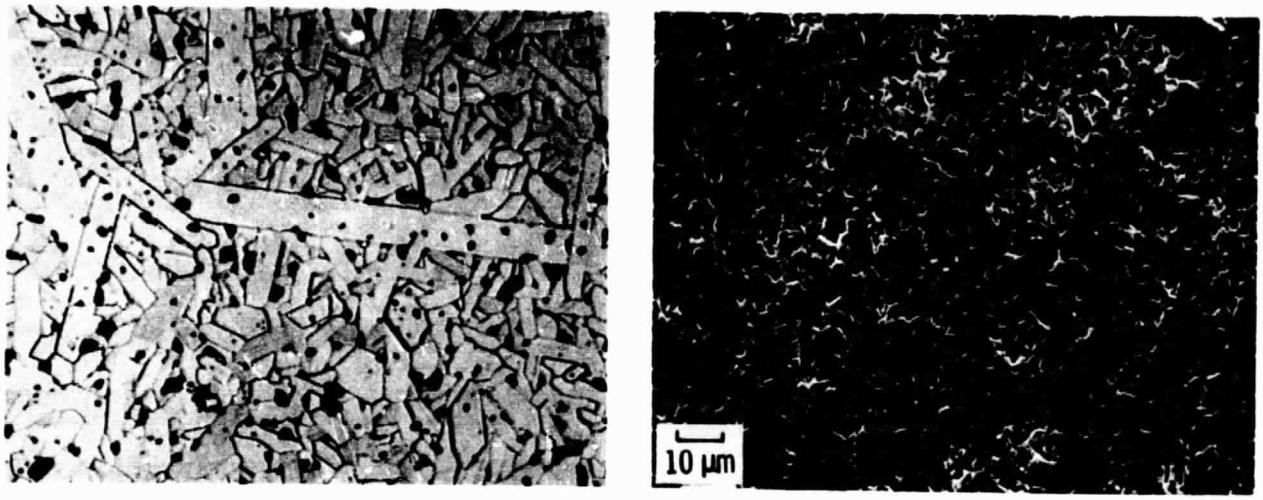

(a) Lenticular and equiaxed grains in a polished and etched sample (optical).

(b) Surface damage after 15µm diamond grinding (SEM).

Figure 1. - Microstructure of as-recieved α-SiC.

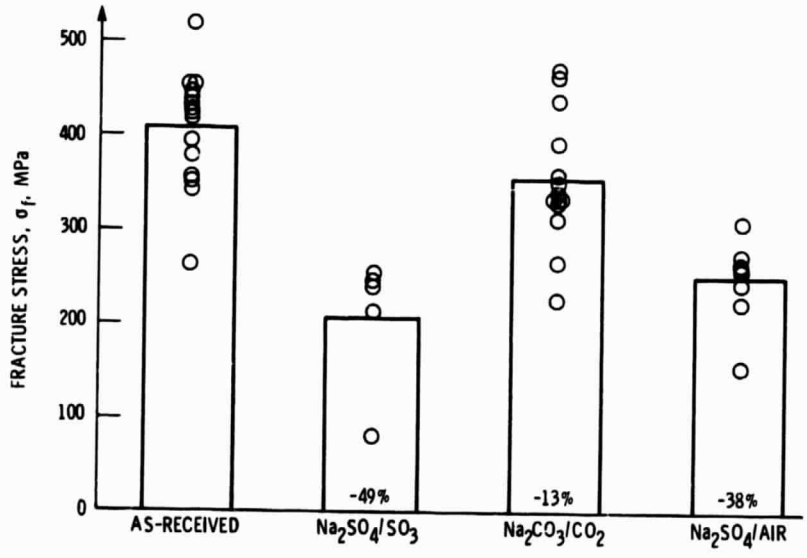

Figure 2. - Effect of 1000 °C/48 hr hot corrosion on 4-pt bend strength of α-SiC; samples ground to 15µm finish before strength test.

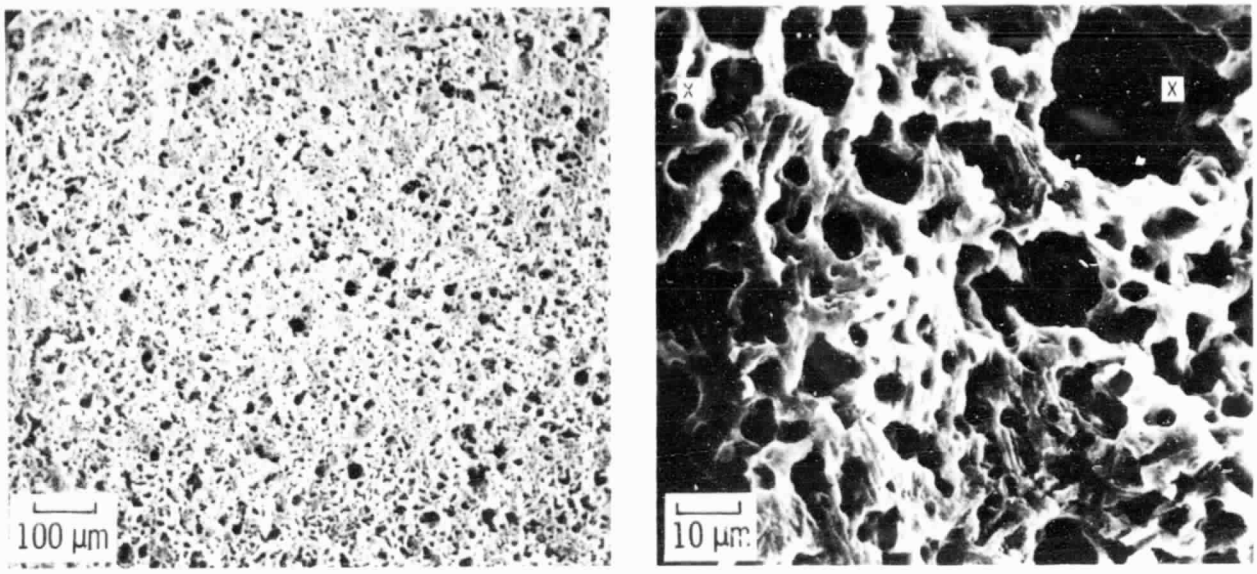

(a) Uniform pitting observed over large areas.

(b) Detail of (a) showing honeycomb pit structure.

Figure 3. - Pitting attack morphology after Na_2SO_4/SO_3 corrosion (scale removed by HF dissolution).

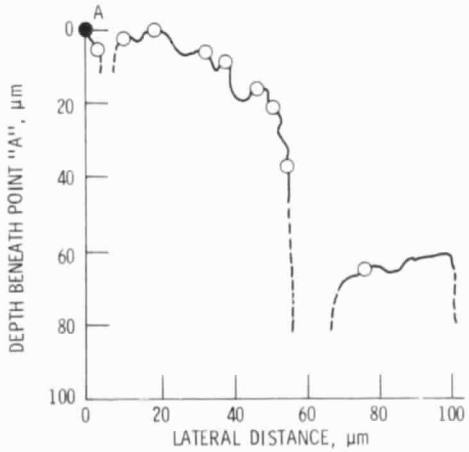

Figure 4. - Pit depth profile obtained across the trace X-X (Fig. 3(b)) by stereopair measurements.

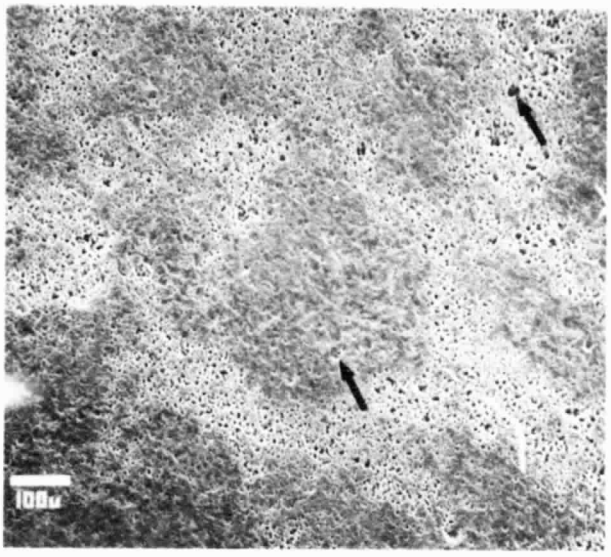

(a) Nonuniform cellular network of pits.

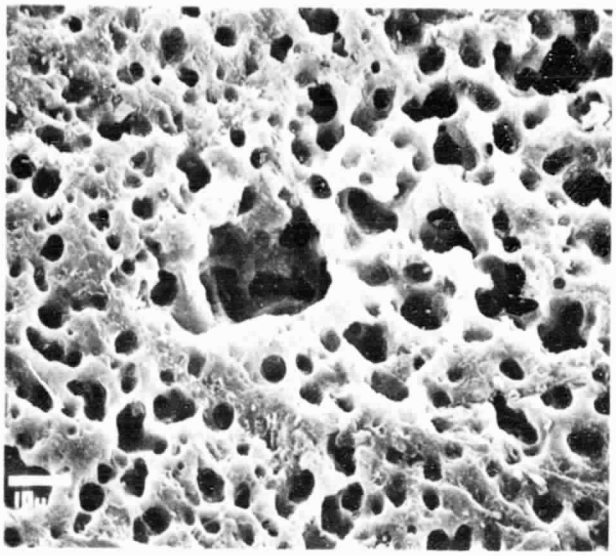

(b) Honeycomb pit structure in a cell boundary.

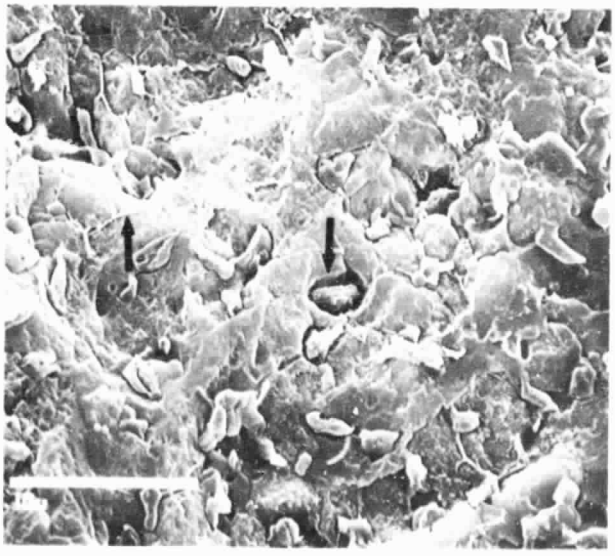

(c) Grain boundary films, inclusions, and absence ofpitting in center of cells.

Figure 5. - Pitting attack morphology after Na_2CO_3/CO_2 corrosion (scale removed by HF dissolution).

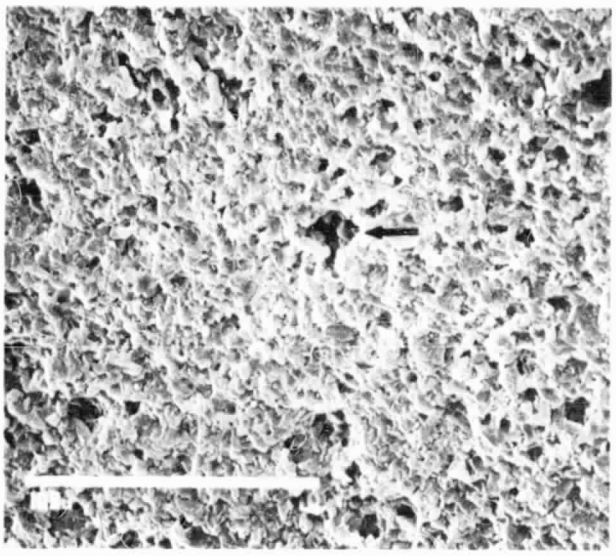

(a) Nonuniform distribution of pits.

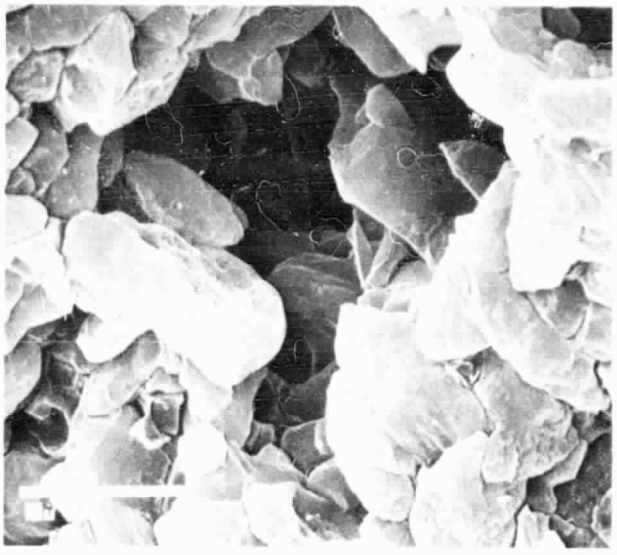

(b) Honeycomb pit structure in deeply pitted region.

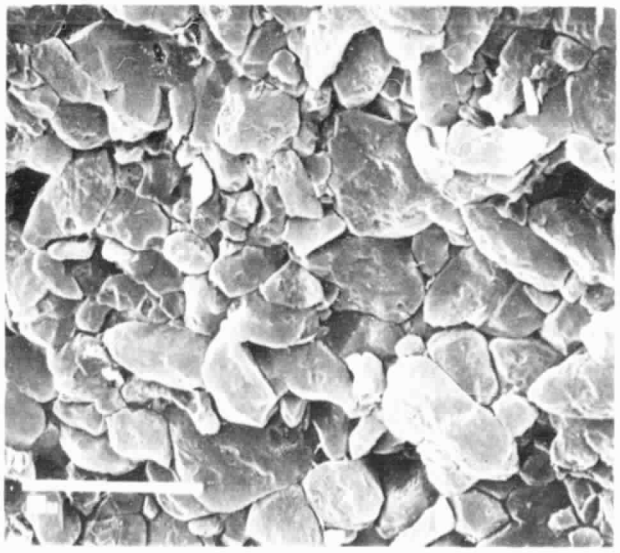

(c) Granular appearance in nonpitted region.

Figure 6. - Pitting attack morphology after Na_2SO_4/Air corrosion (scale removed by HF dissolution).

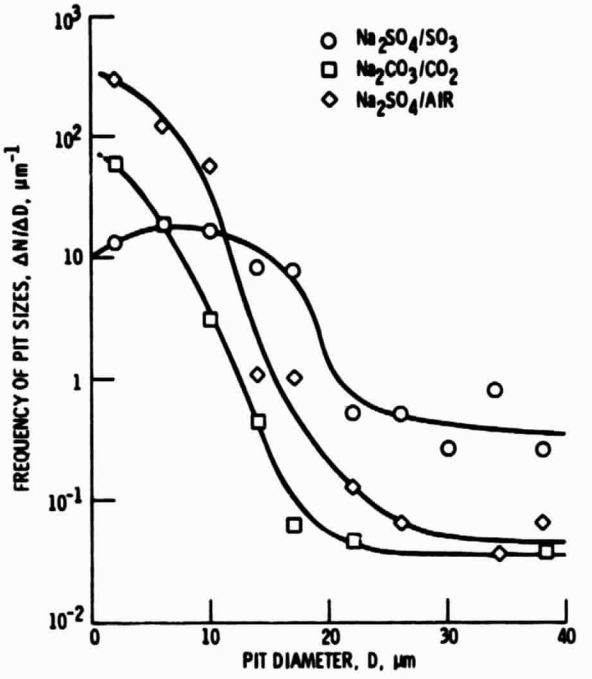

Figure 7. - Histograms of pit diameters for various corrosion conditions, (0.1 mm^2 sampling area; pit diameter interval $\Delta D = 4\mu m$).

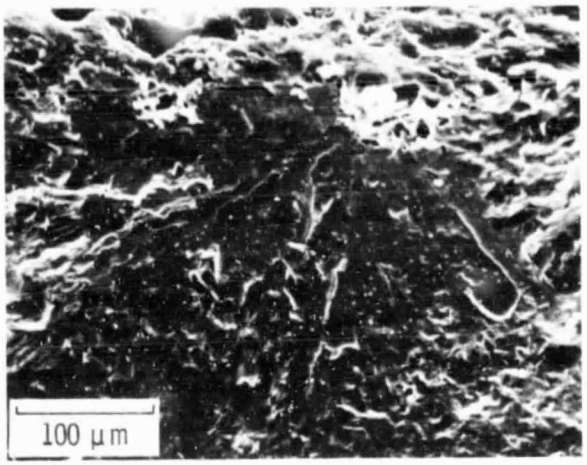

(a) Radial fracture lines in mirror pointing to pit.

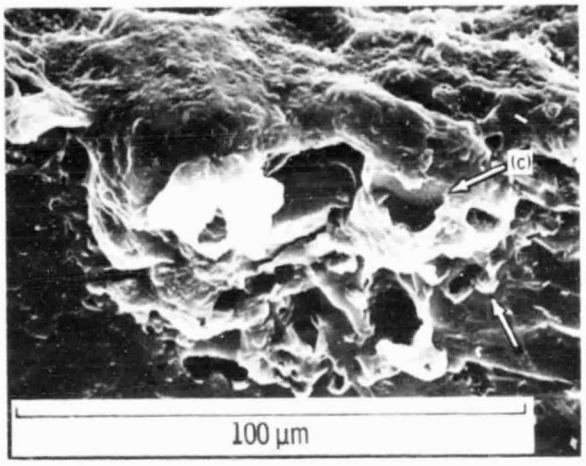

(b) Corrosion pit filled with oxide.

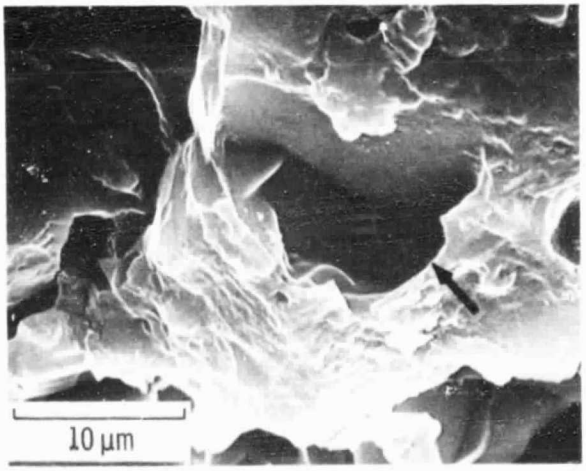

(c) Detail of bubble in scale.

Figure 8. - Corrosion pit fracture origin after Na_2SO_4/SO_3 corrosion (scale polished to 15µm finished before fracture; σ_f = 81 MPa, pit depth = 56µm).

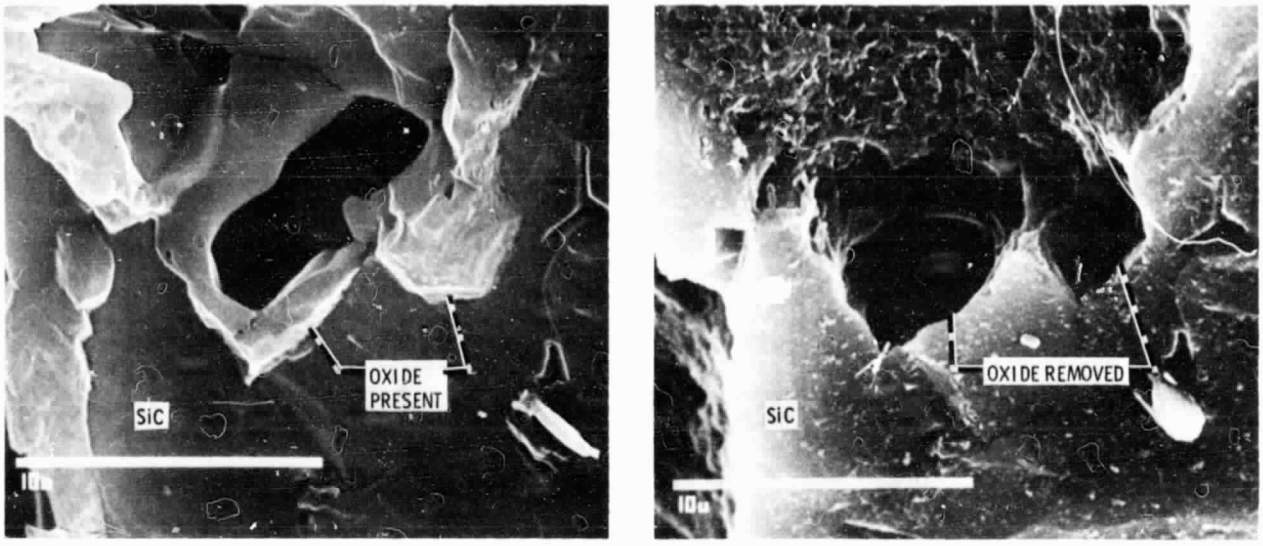

(a) As-fractured.

(b) After scale in pit removed by HF dissolution.

Figure 9. - Bubble formation at the scale-SiC interface (from Fig. 8).

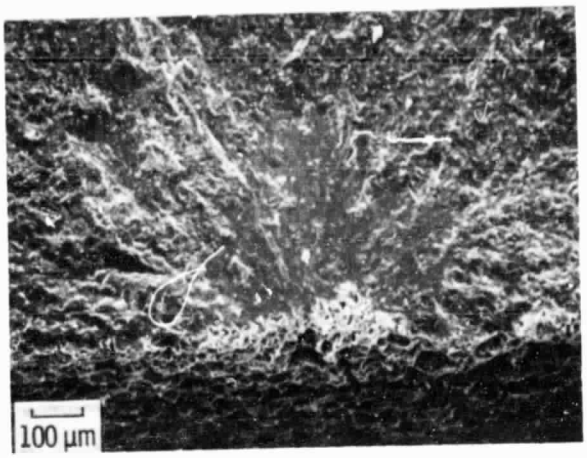

(a) Radial crack lines pointing to origin.

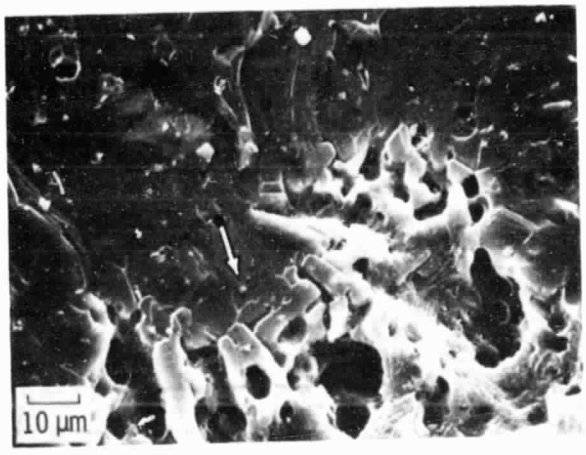

(b) Honeycomb corrosion pit at origin.

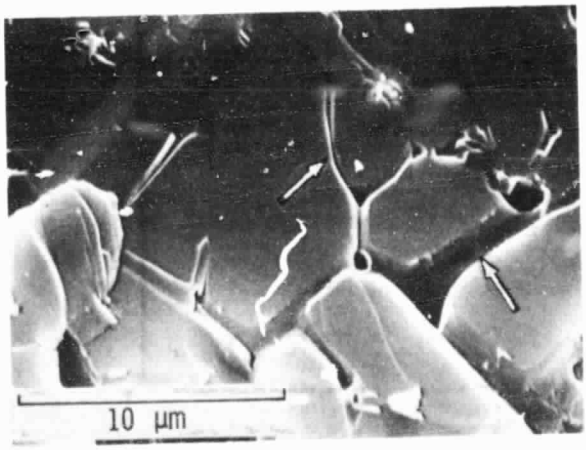

(c) Preferential grain boundary attack ahead of pit (arrow in (b)).

Figure 10. - Corrosion pit fracture origin after Na_2SO_4/SO_3 corrosion (scale removed by HF dissolution; σ_f = 190 MPa, pit depth = 133 µm).

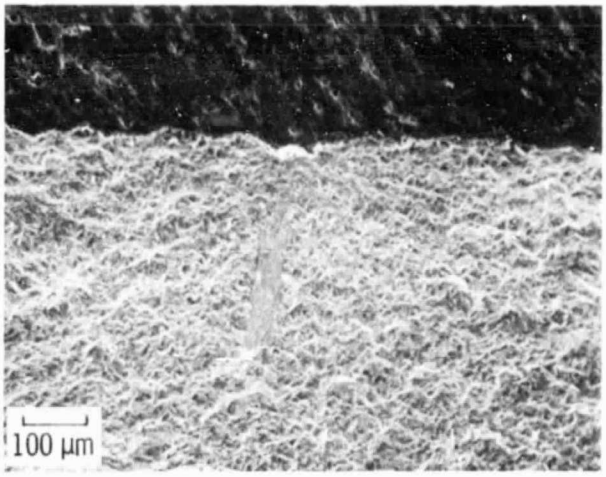

(a) Radial crack lines pointing to origin.

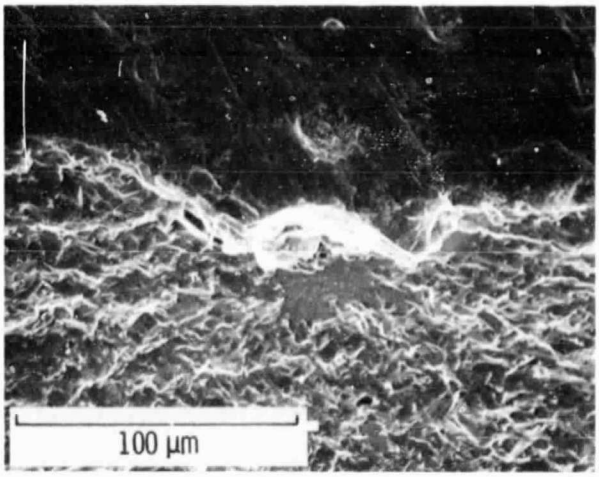

(b) Residual scale overhang at fracture origin.

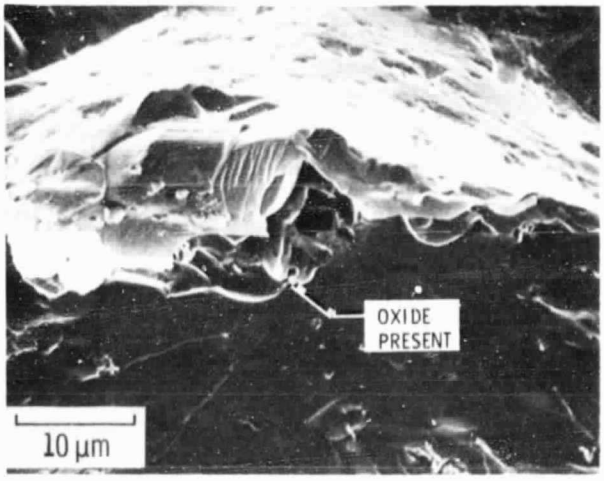

(c) Detail of scale-SiC interface of pit.

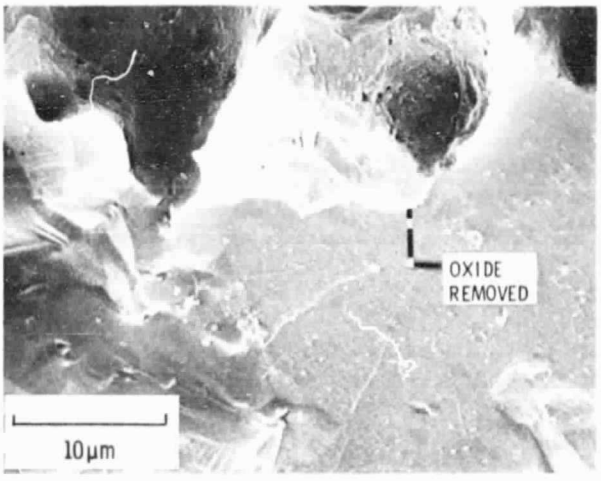

(d) Same as (c) after scale removed by HF.

Figure 11. - Corrosion pit fracture origin after Na_2CO_3/CO_2 corrosion (scale polished to 15μm finished before fracture; $_f$ = 334 MPa, pit depth = 45μm).

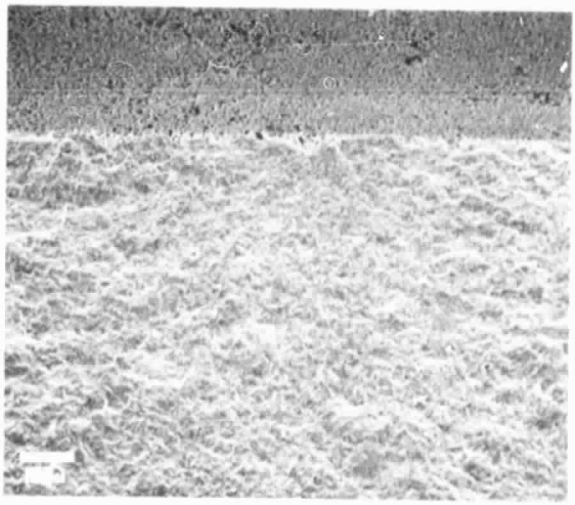

(a) Radial crack lines pointing to corrosion pit.

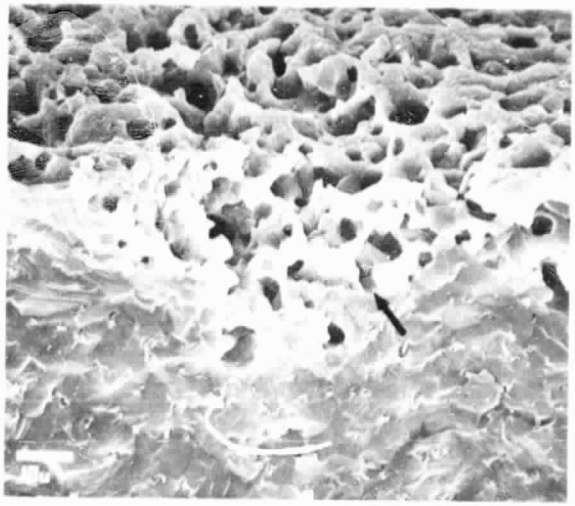

(b) Intersection of deeply pitted region with fracture surface.

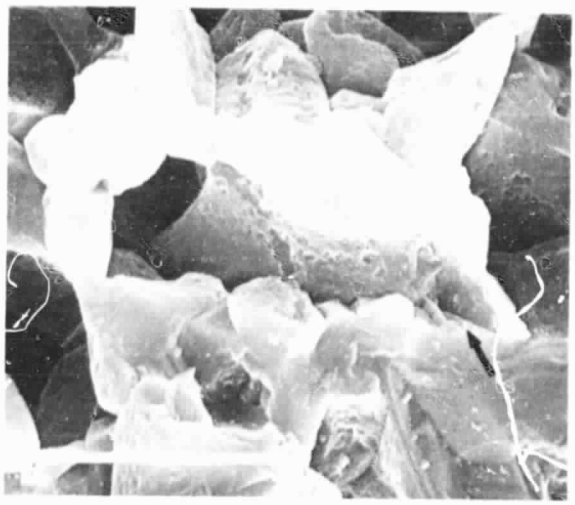

(c) Granular attack morphology in pit.

Figure 12. - Corrosion pit fracture origin after Na_2SO_4/Air corrosion (scale removed by HF dissolution; σ_f = 373 MPa, pit depth = 40 μm).

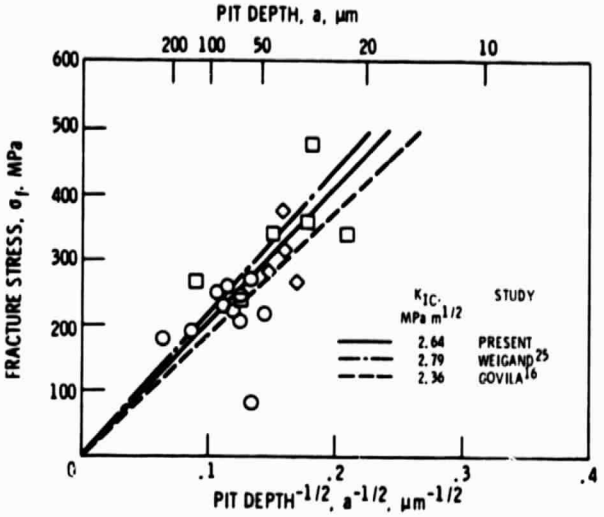

Figure 13. - Correlation of fracture strength with corrosion pit depth; ○ Na_2SO_4/SO_3 corrosion, □Na_2CO_3/CO_2 corrosion, ◇Na_2SO_4/AIR corrosion; lines refer to values predicted assuming semi-circular flaws and K_{IC}'s indicated.

1. Report No.	2. Government Accession No.	3. Recipient's Catalog No.
NASA TM-87052		

4. Title and Subtitle

Mechanism of Strength Degradation for Hot Corrosion of α-SiC

5. Report Date

6. Performing Organization Code

533-05-12

7. Author(s)

James L. Smialek and Nathan S. Jacobson

8. Performing Organization Report No.

E-2507

10. Work Unit No.

9. Performing Organization Name and Address

National Aeronautics and Space Administration
Lewis Research Center
Cleveland, Ohio 44135

11. Contract or Grant No.

13. Type of Report and Period Covered

Technical Memorandum

12. Sponsoring Agency Name and Address

National Aeronautics and Space Administration
Washington, D.C. 20546

14. Sponsoring Agency Code

15. Supplementary Notes

Prepared for The Regional Meeting of the American Ceramic Society, San Francisco, California, October 28-31, 1984.

16. Abstract

Sintered α-SiC was corroded by thin films of Na_2SO_4 and Na_2CO_3 molten salts at 1000 °C. This hot corrosion attack reduced room temperature strengths by as much as 50 percent. Strength degradation was proportional to the degree and uniformity of corrosion pitting attack as controlled by the chemistry of the molten salt. Extensive fractography identified corrosion pits as the most prevalent source of failure. A fracture mechanics treatment of the strength/pit depth relationship produced an average K_{IC} equal to 2.6 $MPa \cdot m^{1/2}$, consistent with published values.

17. Key Words (Suggested by Author(s))

Hot corrosion; Molten salts; SiC; Pitting; Fracture strengths

18. Distribution Statement

Unclassified - unlimited
STAR Category 27

19. Security Classif. (of this report)	20. Security Classif. (of this page)	21. No. of pages	22. Price*
Unclassified	Unclassified		

*For sale by the National Technical Information Service, Springfield, Virginia 22161